ELSEVIER

Journal of Fluids and Structures 24 (2008) 58–74

JOURNAL OF FLUIDS AND STRUCTURES

www.elsevier.com/locate/jfs

Effect of ventricle motion on the dynamic behaviour of chorded mitral valves

P.N. Watton[a], X.Y. Luo[b,*], M. Yin[c], G.M. Bernacca[d], D.J. Wheatley[d]

[a]*Department of Engineering Science, University of Oxford, Oxford, UK*
[b]*Department of Mathematics, University of Glasgow, Glasgow, UK*
[c]*Department of Engineering Mechanics, Xi'an Jiaotong University, Xi'an, PR China*
[d]*Department of Cardiac Surgery, University of Glasgow, Glasgow, UK*

Received 3 May 2006; accepted 25 June 2007
Available online 20 September 2007

Abstract

An Immersed Boundary (IB) model is employed to investigate the dynamic behaviour of a novel chorded mitral prosthesis, which is in the early stages of its development, under physiological flow conditions. *In vivo* magnetic resonance images (MRIs) of the left ventricle are analysed to determine the relative motion of the mitral annulus and the papillary muscle regions of the ventricle. The dynamic boundary conditions are incorporated into IB simulations to test the valve in a more realistic dynamic geometric environment. The IB model has successfully identified the effect of the dynamic boundary conditions on the mechanical behaviour of the valve and revealed the strengths and weaknesses of the current mitral design. The mechanical performance of the prosthesis is compared with recent studies of native porcine valves; differences in mechanical behaviour are observed. Potential improvements for the design of the prosthesis are proposed.

Keywords: Immersed Boundary; Mitral valve; Prosthetic heart valve; Static and dynamic loading; Ventricle motion; Papillary muscle; Fluid–structure interactions

1. Introduction

The left side of the heart accepts oxygenated blood at low pressure from the lungs into the left atrium. The blood then moves to the left ventricle which pumps it forward to the aorta to circulate the body. The heart's valves maintain the unidirectional flow of the blood through the heart, e.g. the mitral valve prevents regurgitation of blood from the left ventricle into the left atrium during ventricular systole and the aortic valve prevents blood flowing back from the aorta into the left ventricle during diastole. The principal fluid phenomena involved in the left ventricular diastolic flow are related to the presence of vortex structures that develop with the strong jet that enters through the mitral valve (Reul et al., 1981; Saber et al., 2001). It is conjectured that the vortex structure has important effects on the function of the ventricle (Bacanni et al., 2003; Daebritz et al., 2003; Pierrakos and Vlachos, 2006).

*Corresponding author. Tel.: +44 141 3304746; fax: +44 141 3304111.
E-mail address: x.y.luo@maths.gla.ac.uk (X.Y. Luo).

0889-9746/$ - see front matter © 2007 Elsevier Ltd. All rights reserved.
doi:10.1016/j.jfluidstructs.2007.06.004

The human mitral valve is a complex anatomical structure consisting of two valve leaflets, an annulus, chordae tendineae, and two papillary muscles which are finger-like projections embedded into the underlying left ventricular myocardium (Chen et al., 2004; Liao and Vesely, 2003). The mitral annulus is a saddle-shaped fibrous ring which seamlessly transitions into the two leaflets (Grashow et al., 2006; van Rijk-Zwikker et al., 1994). The leaflets extend into the left ventricle where they are tethered to the papillary muscles via an intricate arrangement of chordae tendineae (Grashow et al., 2006; Berne and Levy, 1986). The chordae tendineae consist of a complex web of chords that attach all over the leaflets of the valve. They prevent the prolapse of the valve leaflets at systole, and additionally assist in maintaining the geometry and functionality of the ventricle (Komeda et al., 1996a, b). The papillary muscles play an important role and are believed to lengthen during isovolumetric contraction and shorten during ejection as well as during isovolumetric relaxation to maintain the chordae at the same deformation level, during opening and closure (Marzilli et al., 1980).

Normal left ventricular geometry and alignment of the papillary muscles and chordae tendineae prevent mitral valve leaflet prolapse during ventricular systole. Dysfunction of any one or more of these components can cause mitral regurgitation (Grashow et al., 2006; Chen et al., 2004; Redaelli et al., 2001). This may lead to eccentric ventricular hypertrophy, pulmonary oedema and, in instances of acute onset, cardiogenic shock (Grashow et al., 2006). Abnormal stresses on the valve leaflets due to pathological conditions may result in tissue damage and potential valve failure (He et al., 2003). Surgical repair or replacement of the valve is required if valvular function is too poor, or if the condition deteriorates.

If the mitral valve is too severely diseased for surgical repair to be effective, it is generally replaced with a mechanical or bioprosthetic valve (Acar et al., 1994). Although over 50 specific types of replacement valves currently exist, none can be considered an ideal substitute. Mechanical prostheses have suboptimal haemodynamics and promote thromboembolism and blood cell damage, whilst stented prostheses possess limited long-term durability in the mitral position (Yoganathan, 2000).

The development of improved mitral prosthetic valves is an ongoing and costly process. The most ideal replacement should simulate the natural mitral complex as closely as possible. However, to date, all replacement valves in clinical use, mechanical or bioprosthetic, have been designed for the aortic valve position. These valves are simply put in the reversed position for the mitral valve replacement. Potentially, this has significant long-term effects on ventricle pathology due to the loss of functional chordae. The replacement of the asymmetric geometry of the mitral valve by the symmetric aortic valve configuration will also alter the vortex structures that develop as the blood flows through the valve and fills the ventricle. This may have deleterious haemodynamic consequences (Pierrakos and Vlachos, 2006).

In this paper, we simulate a newly designed mitral prosthesis (Wheatley, 2002) using an Immersed Boundary (IB) model (Watton et al., 2007), with an ultimate aim of being able to explore its functionality under a wide range of conditions. It is a polyurethane bileaflet valve, with geometric and mechanical properties emulating (some aspects) of the native mitral valve, with differences related to limitations of synthetic materials. For prosthetic aortic valves developed using this polyurethane material, the mechanical and biostability properties have been extensively tested *in vitro* and *in vivo*, and the performance is very promising (Bernacca et al., 2002; Wheatley et al., 2000). Thus, this mitral valve prosthesis is designed to combine the advantages of both mechanical and bioprosthetic heart valves, i.e. long-term durability without the need for permanent anti-coagulation. However, the polyurethane mitral valve design is considerably more complex than valves designed for the aortic position and extensive, time-consuming tests under wide-ranging conditions are required to verify performance before the valve can be implanted *in vivo*.

The dynamic behaviour of porcine mitral valves has been studied *in vitro* by He et al. (2003, 2005) and Sacks et al. (2002). The Georgia Tech left heart simulator was used to measure surface strains in the valve leaflets under dynamic loading. The effect of the papillary muscle positions on the dynamic strains was also considered. This research provides important insight into the dynamic behaviour of the native mitral valve. Moreover, it enables a benchmark comparison for the performance of our mitral prosthesis.

Both experimental and computational analysis can guide prosthesis design. However, the advantage of a computational model is that material and geometric parameters can be easily changed to determine an optimum design and it enables analysis that may be impractical experimentally. For example, stress and strain distributions can be predicted; the mechanical interaction of the valve leaflets and fluid flow can be simulated in a physiologically realistic environment, e.g. a (prescribed) contracting ventricle. Unfortunately, computational modelling of the native mitral valve is difficult: the geometry of the chordae and leaflets is complex; the dynamic motion of the left ventricle causes a displacement of the papillary muscle base relative to the mitral annulus; the papillary muscles contract and relax during the cardiac cycle; the geometry of the mitral annulus is dynamic. Furthermore, large deformation fluid–structure interactions are present during opening and closing phases. For these reasons, to date, only limited numerical research has been performed on mitral valves compared with aortic valves (Bellhouse, 1969; Ming and Zhen, 1986).

Kunzelmann et al. (1993a, b) developed the first three-dimensional (3-D) finite-element model of the mitral valve using ANSYS. The open and closed mitral apparatus geometry was determined from resin casts of porcine mitral valves. This was used to construct a finite-element model that incorporated all essential anatomical components and regional tissue thickness. Anisotropic material properties were related to the collagen fibre orientation determined from previous studies. The closing phase of the mitral valve was simulated using a physiological time-dependent loading and solved using a quasi-static approach. The model was applied to give extensive further insight into the functioning and malfunctioning of the mitral apparatus, e.g. to consider: the effects of chordal rupture, annular dilatation and leaflet perforation (Kunzelmann et al., 1993a); the effect of replacing chordae tendineae with ePFTE suture (Reimink et al., 1996; Kunzelman and Cocharan, 1993); annular dilatation (Kunzelman et al., 1997); the effect of papillary muscle position on mitral valve function (Cochran and Kunzelman, 1998); flexible versus rigid ring annuloplasty for mitral valve annular dilatation (Kunzelman et al., 1998a); altered collagen concentration in mitral valve leaflets (Kunzelman et al., 1998b). Note that in many of Kunzelman's studies, the papillary muscle tips (which the chordae attached to) were spatially fixed in position relative to a fixed mitral annulus. There is physiological justification for this: the subsequent contraction and motion of the papillary muscles has the effect of fixing the distance between the papillary muscle tips and the mitral annulus plane. Thus the lack of papillary muscle motion in the rigid left ventricular models does reflect the constant papillary muscle tip to annular plane distance.

Einstein et al. (2005) recently developed the first computational model (using LS-DYNA), which accounts for the coupled fluid–structure interactions of the local blood flow and the mitral valve leaflets, during the closing phase of the cycle. The mitral leaflets were modelled as nonlinear membranes and the leaflet material was characterised as an orientated Gaussian distributed population of crimped collagen fibres embedded in an isotropic medium consisting of glycoproteins and elastin. The chordae were modelled as nonlinearly elastic tension cables. The papillary tips were fixed in position relative to the mitral annulus. Symmetry boundary conditions were applied on the septal–lateral midplane to reduce computational cost. The valve was immersed in a domain of Newtonian blood with ventricular and atrial pressure curves applied to the ventricular and atrial surfaces of the blood domain. Model predications showed excellent agreement with available transmitral flow, papillary force and first heart sound acoustic data.

Lim et al. (2005) recently developed the first asymmetric model of the mitral valve complex using ANSYS 5.7 for the whole cardiac cycle. They observed that the motion is highly complex, and involves irregular twisting and skewing and that the annulus and papillary tip motions are 3-D in the atrioventricular chamber. Thus asymmetric boundary conditions are necessary for effective modelling of twisting or pulling of mitral valve. Distance tracings between ultrasound crystals placed in the sheep mitral valve were converted into 3-D coordinates to reconstruct an initial asymmetric mitral model and subsequent boundary conditions. The leaflets were modelled with linear isotropic material properties and uniform thickness. Nonlinear, real time left ventricular and aortic pressure loads were applied synchronously. The quasi-static deformations were determined over one time cycle. This study provided new insight into the distribution of leaflet stress in the mitral valve: in addition to the high leaflet stress that occurs during peak pressure loading, a prominent secondary peak (not observed previously) was observed during isovolumic relaxation of the ventricle. Note this model uses a quasi-static approach to model the valve deformation, i.e. it does not model the fluid–structure interactions.

Watton et al. (2007) modelled the dynamic behaviour of a chorded mitral prosthesis using a purpose developed IB code. The IB model was validated, using IB models of aortic and mitral prostheses, for the static case with ANSYS, and with experiments for the dynamic case. Although discrepancies exist, especially near the contact regions when the mitral valve is closing, good quantitative agreement was achieved using IB. However, in the previous computational simulations, the *chordal attachment points* (CAPs) of the mitral prosthesis were fixed in spatial position relative to the mitral annulus. This was necessary so that the dynamic IB model could be compared with the results from the experimental hydrodynamic function test rig, which uses fixed CAPs.

If the design goes to the *in vivo* testing stage, the chordae of the new mitral valve will be implanted directly through the papillary muscle regions of the ventricle wall and anchored to the external wall of the ventricle, rather than directly to the papillary muscle tips. This will enable the tension of the chordae to be adjusted post-operation to optimise functionality of the valve as well as ensuring secure attachment of the chordae to the heart. As the ventricle continually contracts and relaxes, the CAPs will move relative to the mitral annulus. This additional dynamic motion will undoubtedly affect the dynamic orientations and stretches of the chordae, and therefore the valve deformation and stress distribution. This issue will be explored in this paper.

Modelling the whole ventricle is computationally challenging and unnecessarily time consuming for this initial design stage. Thus we simulate the effect of the motion of the ventricle as the time-dependent boundary conditions for the relative motion of the mitral annulus and the CAPs (which are located in the papillary muscle regions of the ventricle) during the cardiac cycle. This motion is determined by analysing high-resolution magnetic resonance image (MRI) data from a normal human ventricle (obtained from Imperial College).

If this mitral prosthesis were to be implanted, it may restrict the natural dynamic motion of the mitral annulus and papillary muscle regions of the ventricle. This may initiate an undesirable remodelling response of the ventricle. Thus a requirement of this valve design is that it can accommodate the physiological boundary conditions that exist for the native valve between the mitral annulus and the papillary muscle regions of the ventricle wall. Analysis of the MRI data reveals that the relative motion has the largest range perpendicular to the mitral annulus plane and is accompanied by smaller in plane motions. To reduce the complexity of the computational model, a simplification is made: the motion is prescribed perpendicular to the annulus plane. This allows us to explore the mechanical behaviour of the prosthesis in a physiologically more realistic dynamic environment, i.e. study the consequences of attaching the chordae directly into the ventricle wall.

Our model is the first fluid–structure interaction model to consider the whole cycle of the mitral valve, albeit a prosthetic one. It incorporates the dynamic boundary conditions between the papillary muscle regions of the ventricle and the mitral annulus. We consider the effect this motion has on the chordal stretches, the average stretches in the anterior and posterior leaflets, and the pressure gradients across the prosthesis.

2. Method

2.1. The Immersed Boundary method (Peskin, 1972, 1977, 2002; Peskin and McQueen, 1995, 1996; McQueen and Peskin, 1997; Fauci and Peskin, 1988)

The IB method considers the interaction of a viscous incompressible fluid with an immersed system of elastic fibres. The geometry and stiffness of the fibres are constructed to represent the elastic body to be modelled. Each fibre is comprised of a collection of elastic nodal points and connecting elastic fibre segments. The effect of the fibres is to transmit an additional stress to the fluid. A fixed Eulerian lattice, $\mathbf{x} = (x_1,x_2,x_3)$, describes the fluid, and a freely moving Lagrangian lattice, $\mathbf{r} = (r_1,r_2,r_3)$, the elastic material. The interaction between the solid and structure is achieved by distributing an inhomogeneous forcing term onto the fluid domains, and interpolating the velocity of the elastic body from neighbouring fluid nodes near the fluid–structure interface.

Let Ω be the domain of influence or support attached to every immersed elastic nodal point $\mathbf{X}(\mathbf{r},t)$, along a single smooth submerged elastic fibre Γ_s. The elastic fibre point force density $\mathbf{F}(\mathbf{r},t)$ [e.g. Peskin and McQueen (1989)] is

$$\mathbf{F}(\mathbf{r},t) = \frac{\partial}{\partial s}(T\boldsymbol{\tau}), \tag{1}$$

where T represents the tension within the fibre (which may be a nonlinear function of the fibre strain), $\boldsymbol{\tau}$ is the unit tangent vector to the fibres, s is the arc length, and t denotes time. Note, at a typical spatial location A if J fibres pass through the point A, then the nodal force density is

$$\mathbf{F}_A(\mathbf{x},t) = \sum_{j=1}^{J} \mathbf{F}_A^j(\mathbf{r},t) = \sum_{j=1}^{J} \frac{\partial(T_j\boldsymbol{\tau}_A^j)}{\partial s}, \tag{2}$$

where T_j is the tension and $\boldsymbol{\tau}_A^j$ the unit vector of the jth fibre at the point A.

The nodal force density needs to be distributed to the fluid and expressed in terms of the Eulerian variables. This is achieved (Peskin and McQueen, 1989) by expressing it as the convolution of the fibre force density with a delta function:

$$\mathbf{f}(\mathbf{x},t) = \int_{\Gamma_s} \mathbf{F}(\mathbf{r},t)\delta(\mathbf{x} - \mathbf{X}(\mathbf{r},t))\,\mathrm{d}s, \tag{3}$$

where $\mathbf{f}(\mathbf{x},t)$ is the force density applied by the fibre to the fluid at time t and δ is the 3-D Dirac delta function $\delta(\mathbf{x}) = \delta(x_1)\delta(x_2)\delta(x_3)$. The integral is performed over the entire system of fibres.

The Navier–Stokes equations govern the motion of the fibre-reinforced viscous incompressible fluid, i.e.

$$\rho\left(\frac{\partial \mathbf{u}}{\partial t} + \mathbf{u}\cdot\boldsymbol{\nabla}\mathbf{u}\right) + \boldsymbol{\nabla}p = \mu\nabla^2\mathbf{u} + \mathbf{f}, \quad \boldsymbol{\nabla}\cdot\mathbf{u} = 0, \tag{4}$$

where $\mathbf{u}(\mathbf{x},t)$ is the fluid velocity, $p(\mathbf{x},t)$ the fluid pressure, and ρ and μ represent the fluid density and viscosity, respectively. The no-slip condition of a viscous fluid implies that the fibres move at the same velocity as neighbouring fluid particles along the fluid–structure interface and thus

$$\mathbf{u}(\mathbf{X}(\mathbf{r},t)) = \frac{\partial \mathbf{X}(\mathbf{r},t)}{\partial t} = \int \mathbf{u}(\mathbf{x},t)\delta(\mathbf{x} - \mathbf{X}(\mathbf{r},t))\,\mathrm{d}\mathbf{x}, \tag{5}$$

where $\mathbf{u}(\mathbf{X}(\mathbf{r},t))$ is the velocity of the fibres.

Note that Eq. (5) implies that if two nodal elastic points on two different fibres have identical spatial coordinates at $t = 0$, then this will be true for all successive times. Tethering fibres, used to enforce boundary conditions, make use of this fact. These are very stiff, single segment fibres, one end of which (the anchor) has a fixed spatial location, the other end has identical coordinates with the fibre point to be constrained. If the tethered fibre point moves, a stress will be generated in the tethering fibre, acting to oppose the movement of the tethered point. Increasing the stiffness for the tethering fibre, increases the spatial constraint of the tethered nodal point. Note that for the valves to be able to open, current IB computational models require there to be a small gap between the leaflets at all times.

Eqs. (1)–(5) completely specify the system. The incompressible viscous Navier–Stokes equations are discretised on a fixed Eulerian lattice whilst the elastic fibre equations are discretised on a moving Lagrangian array of points, which do not necessarily coincide with the fixed Eulerian mesh points of the fluid computation. The interaction between the fibres and the fluid is handled by a smoothed approximation to the Dirac delta function used to interpolate the fluid velocity to the solid and to apply the solid force to the fluid. The adoption of a regular Eulerian lattice and the periodic boundary conditions enables a Fast Fourier Transform to be employed to solve the fluid equations.

2.2. The mitral valve model

The bileaflet prosthesis is similar to the native mitral valve, with a larger anterior leaflet and a smaller posterior leaflet. The prosthesis incorporates chordae, which originate from the valve annulus and traverse each leaflet, exiting at the leaflet edges to attach to the papillary muscle regions of the ventricle. It is housed on a rigid D-shaped annulus. There are 14 chordae in total, eight in the posterior leaflet and six in the anterior leaflet, extending from the mitral annulus to one of two CAPs. For each CAP, four chordae attach to and run though the surface of the posterior leaflet, and three attach to and run through the surface of the anterior leaflet, see Fig. 1. Note, given that the prosthesis has a rigid annulus, it is not necessary to model the asymmetric dynamic geometry of the native mitral annulus.

The mitral valve prosthesis is designed using the software SOLIDWORKS. Its geometry is exported as an IGES file and imported into GAMBIT, a mesh generator, to produce a finite-element discretisation of the leaflets. The leaflets are divided into sections bordered by each embedded chord and meshed with four node quadrilateral elements. The mesh files (which detail vertices, coordinates and the connectivity matrix for each leaflet) are exported from Gambit to Fortran subroutines to generate an IB fibre network consistent with the geometry and material properties of the leaflets. Briefly, to represent the valve leaflets, each quadrilateral finite element is represented by a cross of four elastic fibre segments which are all attached in the centre of the element and each of the four fibre segments has one end located at

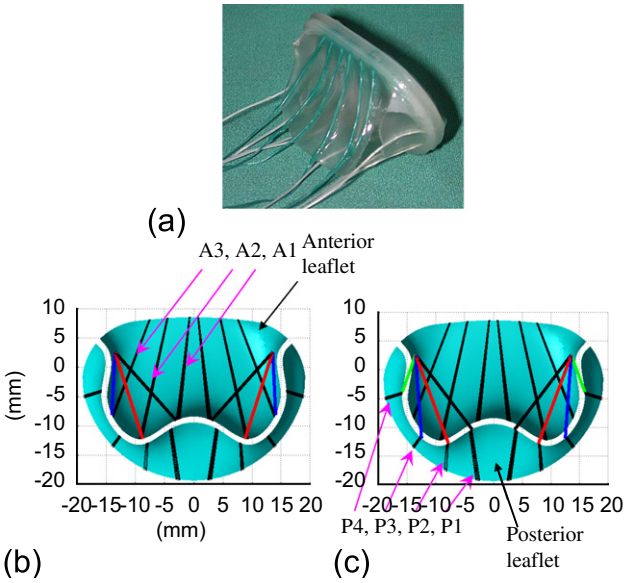

Fig. 1. (a) Photograph of the novel mitral bileaflet prosthesis (side view). The prosthetic valve incorporates chordae which run from the annulus, through the leaflet surface, and leave the leaflet edges to attach to the papillary muscle regions of the ventricle. (b) and (c) The outflow view of the numerical models of the anterior leaflet, and posterior leaflet, respectively. Three chordae attach to each side of the anterior leaflet, denoted A1, A2, A3, and four to each side of the posterior leaflet, denoted P1, P2, P3, P4.

the midpoint of an element edge. The stiffnesses of the fibres are calculated from the thickness and Young's modulus of the material and the size of the element. The embedded chordae are generated from one-dimensional elastic fibre segments; these attach to IB fibre segments which define the leaflets.

For this prosthetic valve, the orientation of the FEM mesh is aligned with the geometry of the embedded chordae in all sections of the anterior and posterior leaflets. Fibre stretches can easily be determined in the directions of the fibres as the material distorts. Here we define longitudinal stretches which are (approximately) parallel to the embedded chordae, and circumferential stretches which are (approximately) perpendicular to the embedded chordae. The exception is within the commissural sections of the anterior and posterior leaflets where due to the complex geometry of the prosthesis, the orientation of the FE mesh (and thus IB fibres) is irregular; thus it is not possible to interpret longitudinal or circumferential stretches here. In these regions, we calculate the maximum of the fibre stretches within each finite-element discretisation of the surface.

Note that a principal stretch may be determined, to correspond to the distortion of the surface, as the fibre network distorts. However, given that the IB model has no resistance to shear, large principal stretches may develop; hence we consider it is more meaningful to only consider stretches in the direction of the IB fibres. More detailed methodology for the fibre generation can be found in Watton et al. (2007).

Each CAP is positioned 53 mm from the mitral annulus plane and slightly inwards from the commissural regions of the prosthesis. The annulus of the valve is spatially fixed. The chordae have a cross-sectional area of $0.4\,\mathrm{mm}^2$ and Young's modulus of 30 MPa. The leaflets have a mean thickness of 0.125 mm, and are modelled as a linear material with a Young's Modulus of 5.4 MPa. Note that for the polyurethane material, the incremental stiffness decreases slowly as a function of stretch. Hence, over the small range of stretches the valve leaflets experience, it seems a reasonable approximation to assume a fixed stiffness (equal to the maximum initial stiffness). The valve leaflets also vary slightly in thickness; this was ignored and a uniform thickness distribution was modelled. These approximations were found to be acceptable: good quantitative agreement was obtained with experimental measurements for a valve subject to static loading for a range of pressures (Watton et al., 2007).

2.3. The Chordal Attachment Point (CAP) motion

The imaging software CMRTOOLS (www.cmrtools.com, Imperial College, UK) is used to analyse high-resolution MRI data of the dynamic motion of the ventricle (32 time slices per cycle). This software enables the user to interactively define the geometry of the ventricle and the directional axes of the papillary muscles at each time step. From the intersection of these coordinate data sets, the papillary muscle regions of the ventricle can be identified. The software Slice-O-Matic is used to track the motion of four points on the mitral annulus plane (marked as a, b, c, d; see Fig. 2). (At the time of this research, CMRTOOLS did not have the facility to track and export the geometry of the mitral annulus.) The geometry data for the ventricle, papillary muscle axes and mitral annulus points is imported into MATLAB to be processed for analysis and visualisation (Fig. 3).

The papillary muscle regions of the ventricle are identified and the relative dynamic spatial variation (x, y, z) of four chosen CAPs (e, f, g, h) located in two papillary muscle regions of the ventricle relative to four marker points (a, b, c, d) on the mitral annulus are analysed (see Fig. 3). Inspection of the MRIs shows that the minimum distance between the mitral annulus and the papillary muscle regions of the ventricle wall occurs in systole. During diastole, the distance increases as the ventricle fills and enlarges and the mitral annulus moves upwards. Note, for the native mitral valve, the papillary muscles contract in systole and relax in diastole, thus helping to maintain a constant distance between the mitral annulus and the papillary muscle tips.

It is observed that the relative motion has the largest range perpendicular to the mitral annulus plane (0–15 mm) and is accompanied by smaller in plane motions (0–5 mm). A simplification is made: only motions perpendicular to the mitral annulus plane are considered in the computational simulations. This is sufficient for us to investigate the mechanical consequences of prescribing a relative dynamic motion, of a physiological magnitude, between the mitral annulus and the CAPs. For example, investigating the effect dynamic boundary conditions have on the average stretches in the leaflets and pressure gradients across the prosthesis during the cardiac cycle. The distance, $d(t)$, between the average position of the four CAPs to the centre point of the mitral annulus plane is determined at each time slice and approximated by an 8-degree polynomial $d(t) = \sum_{i=0}^{8} a_i t^i$, see Fig. 4(a).

2.4. Dynamic IB simulations

A cylindrical tube is constructed from a mesh of azimuthal and axial fibres, see Fig. 5. The valve is positioned $\frac{1}{4}$ of the way down the tube from inflow. The fluid domain is chosen to have $64 \times 32 \times 32$ nodes. Stiff tethering fibres are

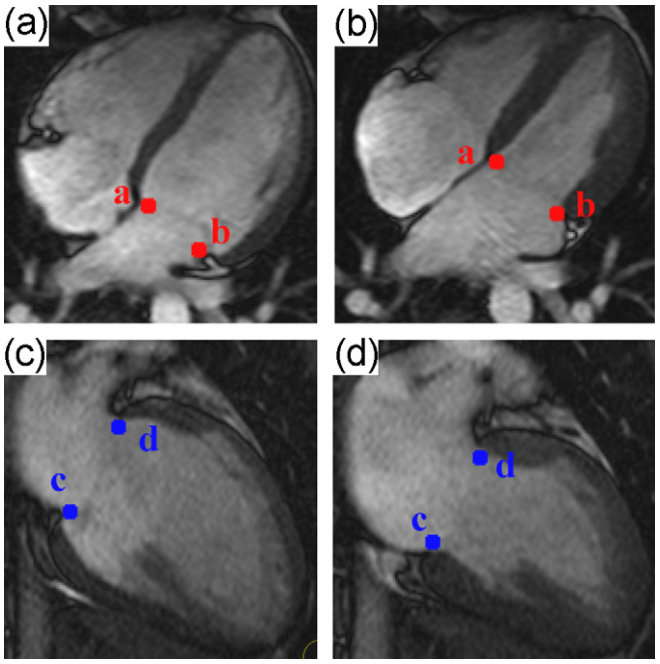

Fig. 2. Slice-o-Matic is used to track the motion of the mitral annulus through two planes of human MRI data. Here illustrated for two different times. A total of 32 time slices are analysed to trace the motion; (a) (b) is the top view of the subject (in horizontal position facing up), and (c) (d) is the (subject's left hand) side view. The four points a, b, c, d, are used to determine the annulus base plane, as in Fig. 3. These four points are clearly identified using the imaging contrast following the mitral valve movements during the cycle. Points are illustrated in red and blue so that the positions can be identified in the 3-D diagram in Fig. 3.

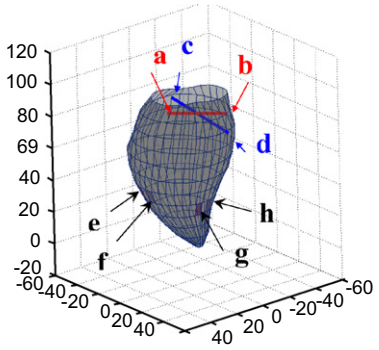

Fig. 3. The data that defines the geometry of the ventricle and papillary muscle (PM) axes and the mitral annulus (MA) marker points is imported into Matlab for analysis. PM regions of the ventricle are identified from the intersection of the PM axes and the ventricle boundary. This enables the dynamic relative motion of the MA and the PM regions of the ventricle to be determined.

attached to all nodal fibre points of the tube and valve housing to render these regions effectively rigid. A periodic physiological velocity profile is prescribed; $u_{\max}(t) = 2F(t)/\pi r^2$, where $u_{\max}(t)$ is the peak velocity of the parabolic flow, r is the radius of the tube and $F(t)$ is a linear interpolation of flow rates recorded from a conventional prosthetic valve hydrodynamic function test rig (Fisher et al., 1986; Mackay et al., 1996). The rig simulates the function of the left ventricle to apply physiological pressure and pulsatile flow conditions to the valves; measuring flow rates through, and pressure gradients across, the valve throughout the cycle. The experimental valve was tested in saline, using the simulated mitral test position. Briefly, a computer-controlled pump generates near-physiological volumetric flows through the ventricular test chamber. The flow input was set at 80 bpm with 80 ml flow volume per pump cycle, at a mean aortic pressure of 95 mmHg.

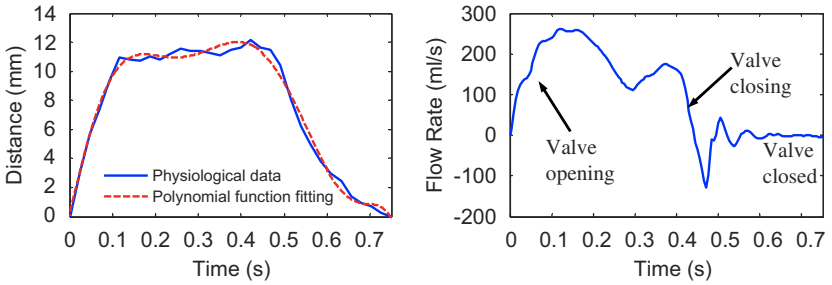

Fig. 4. (a). The relative motion of the papillary muscle regions of the ventricle and the centre of the mitral annulus plane is determined from physiological data and approximated by a polynomial function. This graph illustrates the variation in the distance, i.e. $d(t)-d(0)$. It can be seen that at the onset of ventricular filling ($t=0$), the relative distance between the mitral annulus and CAPs is a minimum, this increases as the ventricle fills and the mitral annulus moves upwards, it remains fairly constant and then decreases again during systole. (b) The prescribed flow rate.

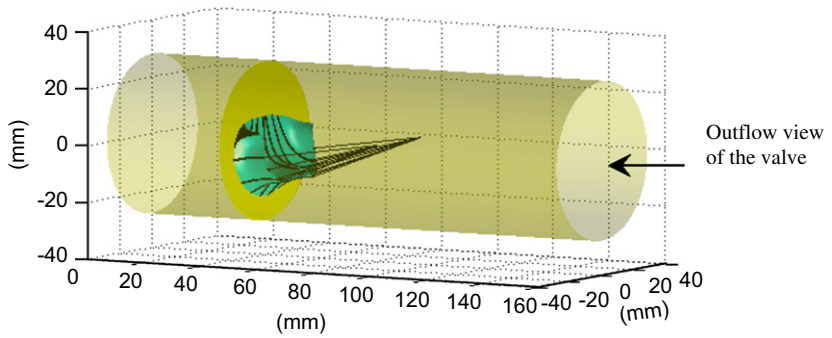

Fig. 5. The valve is housed in a cylindrical tube and subject to period velocity boundary conditions. The outflow view looks down along the axis of the cylinder as in Fig. 1(b and c).

Fig. 4(b) illustrates the experimental flow rate though the mitral valve which is prescribed in the IB simulations. In these simulations, $t=0$, denotes the beginning of the dynamic opening of the valve, flow reduces to zero at around 0.45 s and the maximum systolic pressure occurs around 0.5 s. Note that the flow rate is negative when the valve is closing. This is the closing volume, which is a negative flow cause by the movement of the mitral valve leaflets closing. Some small valve leakage may contribute to this volume when the valve is closed. Promisingly, the closing volume of the prosthesis is of the same order of magnitude of that observed for the native valve [e.g. compared with He et al. (2005)].

All computations were executed on Titania, the White Rose Grid Computing node housed at Sheffield University; a cluster of ten identical (Model V880) machines, each of which comprises eight 900 MHz UltraSparc processors configured in shared memory architecture. MATLAB scripts were written for graphical post-processing.

3. Results

3.1. The dynamic cycle of the mitral valve with the CAP motion

The simulation is performed for one complete cycle, i.e. 0.75 s, beginning at the onset of ventricular diastole. A synchronous periodic CAP motion is prescribed with one cycle lasting 0.75 s. Fig. 6 shows the dynamic behaviour of the valve for a full cycle. The colourmap illustrates the maximum fibre stretches within each finite-element section of the valve leaflet surface. The opening of the valve occurs between 0 and 0.1 s; closure between 0.45 and 0.55 s, i.e. valve closing and opening durations are both around 0.1 s. This is comparable with the data from native mitral valve measurements: documented opening/closing durations are 0.075 s/0.1 s and 0.1 s/0.15 s from He et al. (2003) and (2005), respectively.

The anterior leaflet is reasonably insensitive to CAP motion, i.e. it can accommodate the relative motion of the mitral annulus and CAP. However, the posterior leaflet is subject to significantly increased stretches (up to 1.2), compared to

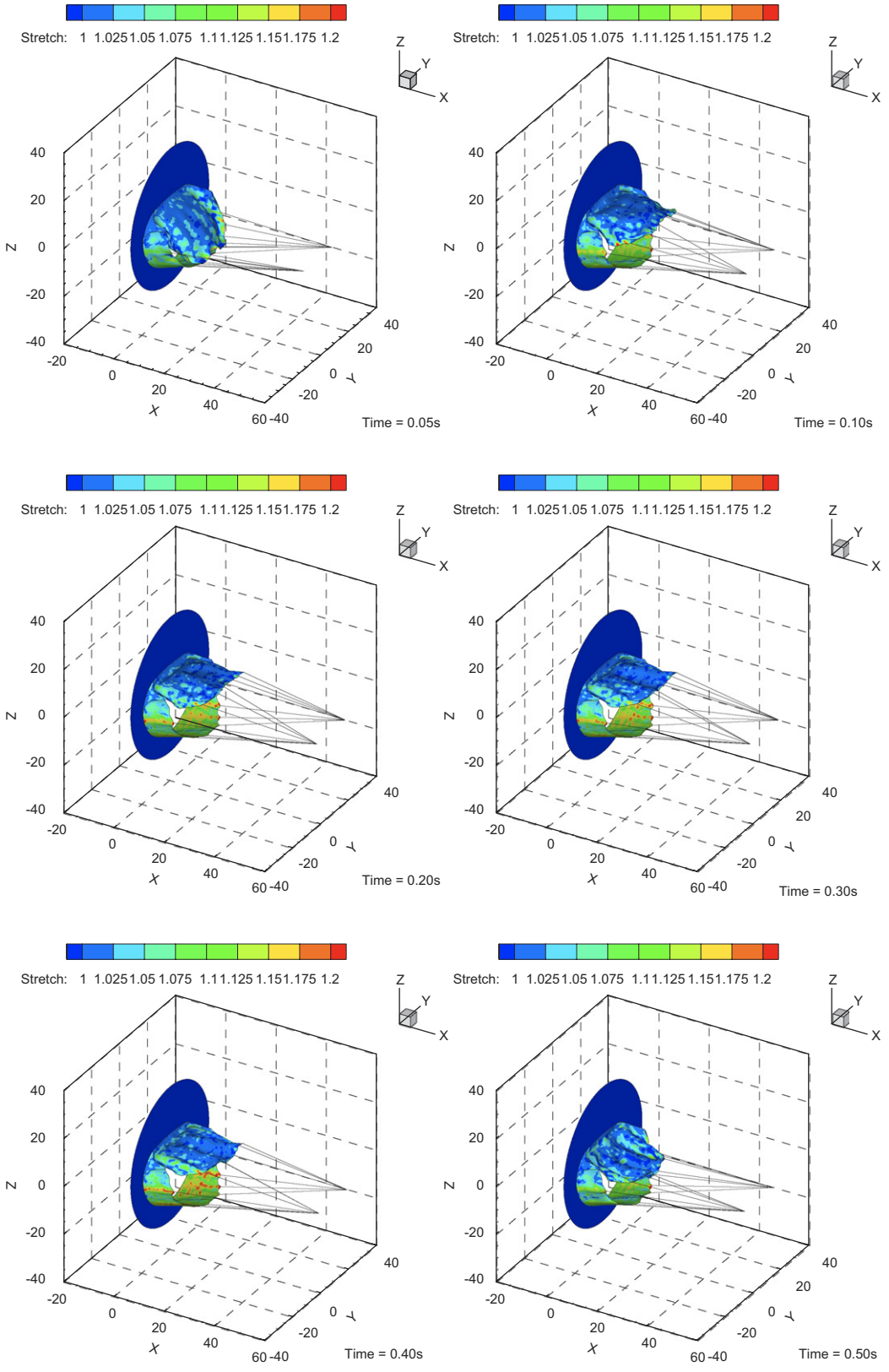

Fig. 6. A complete dynamic cycle of the chorded mitral prosthesis with prescribed CAP motion. The colour scale shows the magnitude of maximum fibre stretches across the surface of the valve leaflets. Note the posterior leaflet is subject to the greatest stretches.

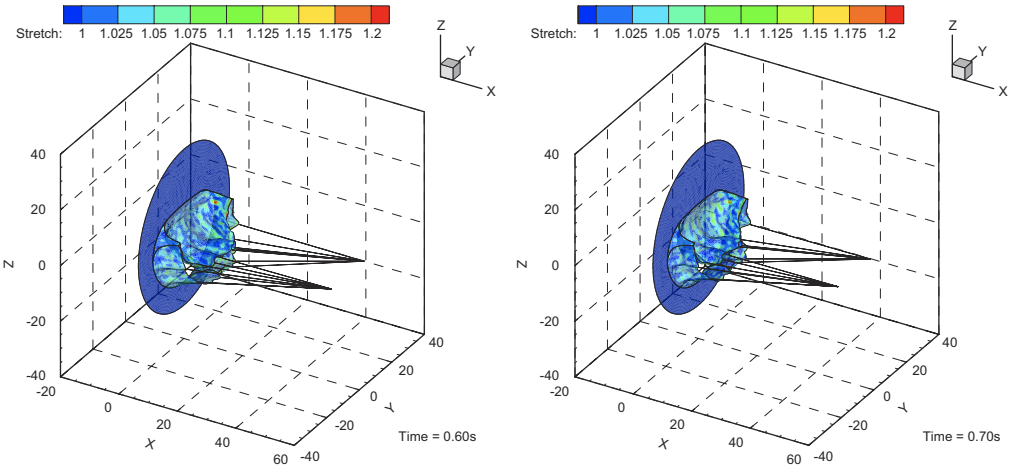

Fig. 6. (*Continued*)

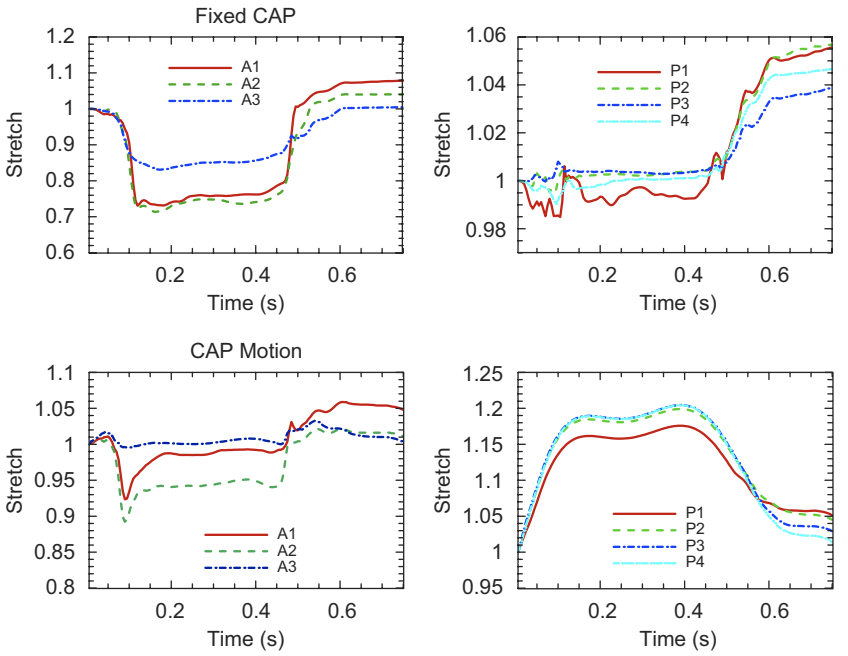

Fig. 7. Stretches of the chordae for no prescribed CAP motion (top) and prescribed CAP motion (bottom). Left diagrams show chordae attached to the anterior leaflet; right diagrams, chordae attached to the posterior leaflet.

the example with no CAP motion. This may be attributed to the limited range of motion of the posterior leaflet for this prosthesis design. This effect is highlighted by examining the stretches in the chordae in Fig. 7.

The variations of stretch with time in the anterior and posterior chordae with and without CAP motions are shown in Fig. 7. Without the CAP motion, the anterior chordae are relaxed during the opening of the valve and it is only at systole when they become taut. The behaviour of the posterior chordae is more complex. During the initial stage of opening, they oscillate between being taut and relaxed. Once the valve has opened (after approximately 0.1 s) they remain slightly taut until systole, when the stretches rapidly increase up to 1.01–1.04. With the inclusion of the dynamic CAP motion in the computational simulations, it can be seen that during the first 0.05 s of opening, both anterior and posterior chordae are taut, indicating that the CAP motion facilitates the opening of the valve, i.e. the chordae are assisting pulling the leaflets apart. As the valve opens, due to the relatively large motion of the anterior leaflet, only one

chorde (A3) remains slightly taut. However, all four posterior chordae are significantly taut (stretches of approximately 1.2) throughout the simulation.

3.2. Effects of CAP motion on pressure gradients across the prosthesis

The pressure gradients across the prosthesis are illustrated in Fig. 8. The maximum opening pressure gradient reduces from 28 mmHg (without CAP motion) to 12 mmHg (with the CAP motion). Thus CAP motion significantly facilitates the opening of the valve. Once the valve is opened for both simulations, the pressure gradients fall to around 3–4 mmHg. This agrees with the experimental value measured during this phase. Note that the pressure gradient without CAP motion remains slightly higher than that with CAP motion before the valve is closed.

3.3. Effects of CAP motion on average strains within the leaflets

To demonstrate the influence of the CAP motion on the whole mitral valve, the average stretches (over a section of the surface) during the dynamic cycle of the valve are considered within three regions of the anterior and posterior

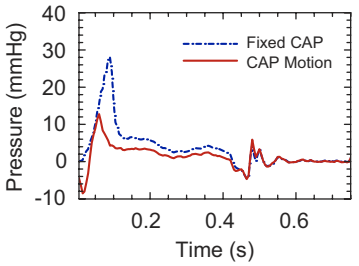

Fig. 8. Pressure gradients across the mitral prosthesis with (solid) and without (dotted) the CAP motion.

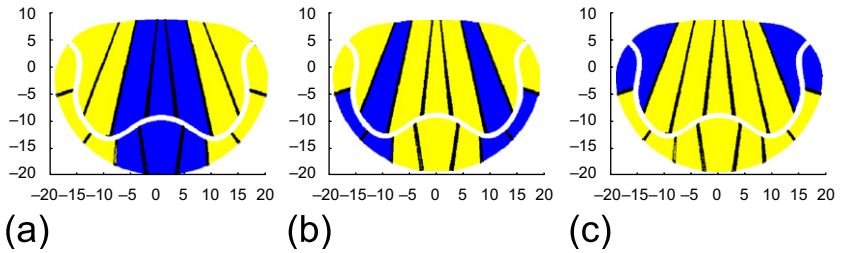

Fig. 9. Regions defined for studying stretches in different areas. The darker areas indicate (a) the central, (b) off-central, and (c) commissural regions of the mitral leaflets.

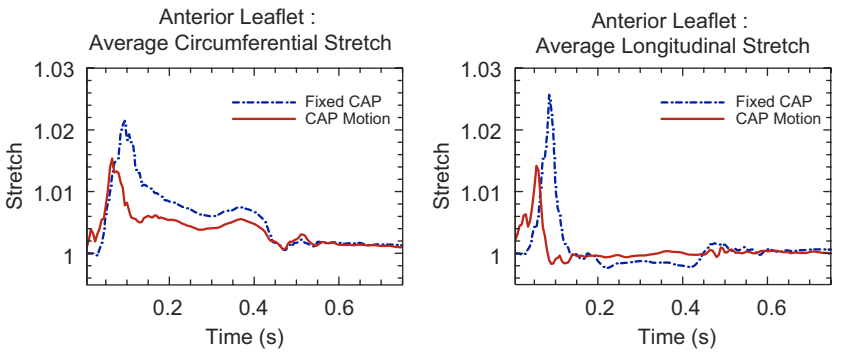

Fig. 10. Surface average of circumferential and longitudinal stretches in the central region of the anterior leaflet.

leaflets: namely, *central*, *off-central* and *commissural* regions of the leaflets (see Fig. 9). In the central and off-central regions both longitudinal (following the direction of chordae) and circumferential stretches are analysed. In the commissural regions of the leaflets, the surface average of the maximum fibre stretch in each element is determined.

3.3.1. Stretch analysis: central region

In general, it is seen that the stretches in the central region of the anterior leaflet are affected by CAP motion in the similar way as in pressure gradients, though to a smaller scale, see Fig. 10. The inclusion of CAP motion reduces the maximum values of both circumferential and longitudinal stretches, i.e. from 1.022 to 1.015, and 1.026 to 1.014, respectively. This is attributed to the motion of the CAP, pulling on the chordae, and assisting the opening of the leaflets. It can be seen that for no CAP motion, the circumferential stretch remains at slightly higher values throughout, i.e. 1.01, compared with cases with CAP motion (approximately 1.005). Both longitudinal and circumferential stretches

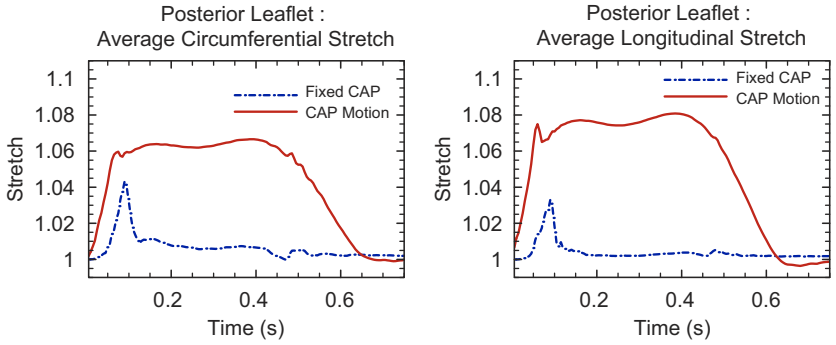

Fig. 11. Surface average of circumferential and longitudinal stretches in the central region of the posterior leaflet.

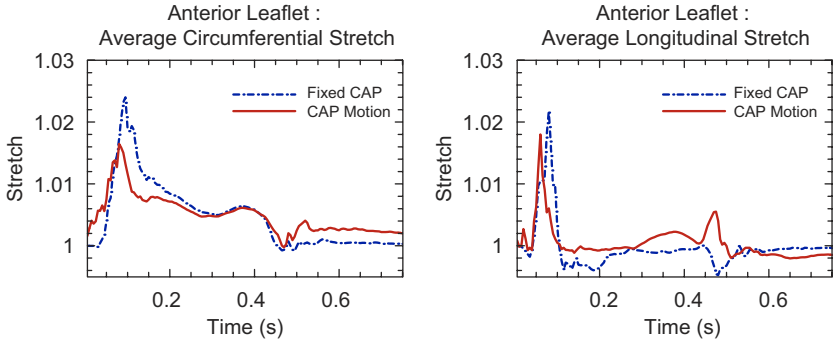

Fig. 12. Surface average circumferential and longitudinal stretches in the off-central region of the anterior leaflet.

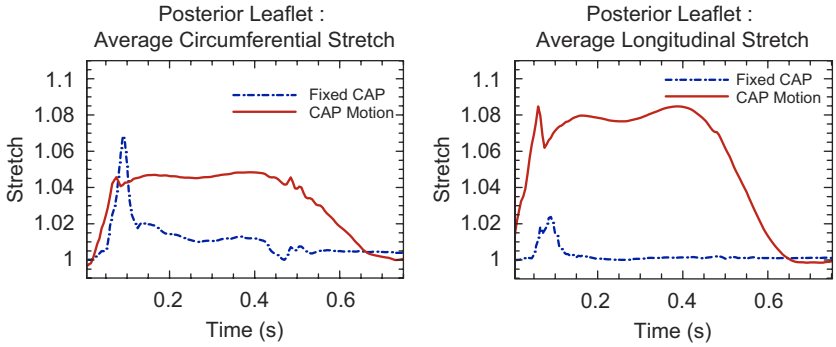

Fig. 13. Surface average circumferential and longitudinal stretches in the off-central region of the posterior leaflet.

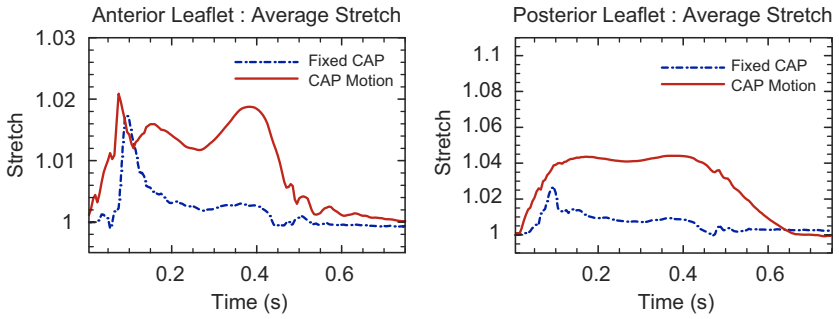

Fig. 14. Surface average of maximum stretches in the commissural regions of the anterior leaflet and posterior leaflets.

remain close to 1 once the valve is opened. In general, there is no significant difference for anterior leaflet when CAP motion is activated.

The central region of the posterior leaflet, on the other hand, is much more significantly affected by CAP motion (see Fig. 11). With no CAP motion, the stretches initially increase rapidly and then reduce following leaflet opening. The inclusion of CAP motion results in considerably higher circumferential and longitudinal stretches throughout most of the dynamic cycle. The circumferential stretches increase to 1.062 and longitudinal stretches to more than 1.08.

3.3.2. Stretch analysis: off-central region

The pattern of the average stretches in the off-central region of the leaflets is similar to that of the central region, see Figs. 12 and 13, i.e. the over-stretch with CAP motion is observed specially in the posterior leaflet.

3.3.3. Stretch analysis: commissural regions

With CAP motion, the average stretch is higher for both the anterior and posterior leaflets, for most part of the cycle, although to a lesser degree compared to the other regions of the posterior leaflet (see Fig. 14).

4. Discussion

It is of interest to compare the mechanical behaviour of our prosthesis with a native valve. First though, let us reiterate the objectives of the valve design. The prosthesis should not restrict the natural dynamic boundary conditions that exist between the papillary muscle regions of the ventricle wall and the mitral annulus. The current design has shown large stretches in the posterior leaflet and chordae when subject to such boundary conditions. Hence if it was implanted it would restrict the natural boundary conditions—consequently, this may have a detrimental effect on the long-term durability of the valve and on ventricular function. Our simulations suggest that modifications might improve the performance of our prosthesis design.

In the simulation with CAP motion a major difference is observed compared with the mechanical behaviour of the native valve. Maximum stretches in both the valve and chordae in the native porcine valve occur when the valve is closed, i.e. in systole, whilst in our dynamic simulation with CAP motion, the maximum stretches occur when the valve is opened. In He et al.'s (2003) experiments, the papillary tips are fixed in position relative to the mitral annulus, this should be considered when making comparisons with our simulations. In fact, to make consistent comparisons here, we consider the numerical dynamic simulation with no CAP motion.

Native valves display a considerable degree of anisotropy. He et al. (2003, 2005) have analysed the dynamic stretch behaviour of porcine mitral valves and find mean systolic longitudinal and circumferential stretches for the anterior leaflet to be 1.29 and 1.08 (He et al., 2003) and 1.23 and 1.025 (He et al., 2005) for the posterior leaflet; i.e. the longitudinal stretches are approximately 1.2 times greater than circumferential stretches. In IB computational analysis (with no CAP motion), at systole, the average longitudinal and circumferential stretches of the anterior leaflet are 1.012 and 1.01, and for the posterior leaflet are 1.018 and 1.01. Clearly, the prosthesis is stiffer than the native valve and only marginally greater longitudinal stretches are observed. However, the embedded chordae currently reinforce the prosthesis design in the longitudinal direction. If the chordae reinforced the leaflets circumferentially, similar anisotropic stretch behaviour may be observed: alternative geometric arrangements of chordae may be implemented in future valve designs.

Ritchie et al. (2006) measured the stretches of the porcine mitral valve chordae under physiological loading conditions. They observed the maximum stretches for posterior and anterior chordae are in the range of 1.043–1.057, which are similar to the maximum stretches of the anterior chordae predicted for the prosthesis, i.e. up to 1.04.

The prosthesis has maximum leaflet and chordae stresses of approximately 1.1 and 1.2 MPa, respectively. Although these values are below the ultimate tensile stress values of 28.6 and 71.7 MPa respectively[1], it is well recognised that valve failure is not directly related to ultimate stress of leaflet materials and fatigue factors are usually more important (Bernacca et al., 1995, 1996, 1997). Furthermore, whilst the stresses are below ultimate tensile stress limits, the most likely cause of valve failure for this design will arise from the fracture or detachment of the chordae from the leaflet matrix.

A major difference between the native valve and the mitral prosthesis, is that the function of the papillary muscles is lost. In theory, it may be possible for the prosthetic valve to be attached to the papillary muscle tips, rather than directly into the papillary muscle regions of the ventricle wall. However, in clinical practice, it is highly difficult to attach the valve directly to the papillary muscles without damaging them and the risk of failure of the chordal attachment would be increased with unacceptable consequences for valve recipients. Furthermore, it is not clear if the papillary muscles will still function when they are detached from the native mitral valve leaflets.

The best materials available to us currently are still greatly inferior to the material of the native valve apparatus. Therefore, even if the designs are made to look and function like the native valves, some essential modifications are unavoidable to account for the material differences. The same is true for bioprosthetic aortic designs (Vesely, 2003). Furthermore in our design the functional role of the papillary muscles is not present. Given that a mitral prosthesis must be "fail safe" and function without the mechanical role of the papillary muscles, and given the constraints of available materials, some deviations of the valve design from the physiology of the native mitral valve apparatus will be necessary. In fact, although the prosthetic design is roughly based on that of the native valve, there are some significant material and geometric differences to native (porcine) valves (Einstein et al., 2005): here the leaflet thickness is 0.125 mm, compared to the porcine mitral valve thickness of 1.26 mm; the Young's modulus is 5.4 MPa whilst the porcine mitral valve's Young's modulus varies between 0.83 and 9 MPa (Lim et al., 2005).

Based on our simulations, some approaches to improving the current design are suggested:

(i) Modifications to the geometry of the design to allow a greater movement of the posterior leaflet.
(ii) Exploring the possibility of attaching the posterior chordae to a different region of the ventricle so that the relative motion of the mitral annulus and the posterior CAPs is not so great. Here though, one would have to be sure that the leaflets still coapt well, particularly if the ventricle remodels following the implantation of the valve.
(iii) Designing a stiffer posterior leaflet which does not require chordae. Here the anterior leaflet chordae would still play the role of maintaining the functionality of the ventricle, i.e. preventing the distension. However, the flexible posterior leaflet is desirable to help prevent regions of stagnant blood flow.
(iv) Possibly modifying the elasticity of the chordae which attach to the posterior leaflet, i.e. use low-modulus external chordae that can accommodate high strains, and high-modulus internal chordae, which resist deformation. This may be an option provided that a material can be found for the chordae that can undergo large strains whilst maintaining durability.

The IB method has enabled us to explore the practicality of the current design, without the need for experimental simulations. Future developments of this design can be tested with IB modelling; once a satisfactory design is developed, it can be tested extensively in an experimental rig. However, limitations of the IB method also need to be addressed. The valve is modelled as a network of spring-like fibres, thus no bending or shear effects are modelled. This causes inaccuracy of the mitral valve deformation during opening and particularly closing. Thus the model, in its present form, cannot be used to estimate the valve leakage reliably, nor can it model the contact problem effectively and accurately predict the deformation of the valve in the maximum pressurised state. A small separation must exist between leaflets to enable them to separate. If the fluid grid does not have a sufficient resolution between the leaflets, a "sticking effect" occurs. A consequence of this is that during valve opening, an artificially higher opening pressure may be required to open the valve (Watton et al., 2007). Currently, a uniform fluid grid is employed which enables the governing equations to be solved efficiently using Fast Fourier Transforms. However, this does not allow local mesh refinement. To improve the computational accuracy, employing a numerical scheme that utilises an adaptive mesh is desirable. In summary, the IB method needs to be improved to model bending stiffness and the contact problem effectively.

[1]Data from http://www.polymertech.com/materials/bionate.html#Properties

Although the CAP motion seems to help the valve to open by reducing the opening pressure by almost two thirds, the opening pressure gradient still appears somewhat higher than that of the native valve, i.e. the opening pressure gradient is about 3 mmHg for the native valve (He et al., 2003), whilst our valve requires 12 mmHg with CAP motion and 28 mmHg without CAP motion. However, the peak opening pressure gradient spike, which is observed in both the IB model and in experiment, is an artefact of the lack of compliance in the rigid chambers of the experimental test rig (Fisher et al., 1986) and the IB computational tube. If the valve was actually implanted *in vivo* (or in a compliant computational ventricle), there would be a more compliant response and thus the spike would be less pronounced. A suitable measure indicative of expected valve performance in the clinical context is the mean pressure gradient across the valve taken from the start of forward pressure to the end of forward pressure (Bernacca et al., 2004; Mackay, 1992). Promisingly, experimental results with fixed CAP motion show that the *mean* pressure gradient for our prosthesis is 3–4 mmHg—this is consistent with predictions from IB.

Finally, it is worth mentioning that many issues discussed here are also encountered in the modelling of aortic valves. For example, the necessity of accurately modelling the anisotropic nature of the valve (Liu et al., 2007); the sensitivity of the stress distributions to the geometry of the valve, in particular, location and magnitude of the maximum stress (Christie, 1992); the need to alter designs for surgical considerations, or to compensate for the fact that bioprosthetic material is inferior to native tissues (Vesely, 2003; Yoganathan et al., 2005).

5. Conclusion

The IB method is successfully employed to assess the design of the chorded mitral prosthesis, with the effect of the ventricle motion considered. The dynamic boundary conditions were determined from human *in vivo* MRI data, and the IB method was applied to solve the large deformation, fluid–structure interactive, time-dependent problem.

The analysis of MRI data has enabled the relative motion of the mitral annulus and the papillary muscle regions of the ventricle to be determined. Potentially, this motion could be incorporated into experimental simulations. However, at this stage it is more cost-effective and straightforward to analyse the effect of this motion with computational analysis.

Dynamic analysis suggests that the chordae act to reduce the pressure gradients required to open the valve, and thus they assist in the opening of the valve leaflets. It is seen that the motion of the anterior leaflet can accommodate the large relative motion between the mitral annulus and CAPs on the ventricle wall. However, the current design results in an over-stretching of the posterior leaflet. The simulations successfully predicted the dynamic performance of the novel mitral design and suggested potential improvements in future designs.

Acknowledgement

Funding from the Royal Society of London (REF. Q816) is gratefully acknowledged.

References

Acar, C., Farge, A., Ramsheyi, J.C., Chacgques, J.C., Mihaileanu, S., Gouezo, R., Gerota, J., Carpentier, A.F., 1994. Mitral valve replacement using a cryopreserved mitral homograft. Annals of Thoracic Surgery 57 (3), 746–748.

Bacanni, B., Domenichini, F., Pedrizzetti, G., 2003. Model and influence of mitral valve opening during the left ventricular filling. Journal of Biomechanics 36 (3), 355–361.

Bellhouse, B.J., Bellhouse, F.H., 1969. Fluid mechanics of the mitral valve. Nature (London) 224, 615–618.

Bernacca, G.M., Mackay, T.G., Wilkinson, R., Wheatley, D.J., 1995. Calcification and fatigue failure in a polyurethane heart valve. Biomaterials 16 (4), 279–285.

Bernacca, G.M., Mackay, T.G., Wheatley, D.J., 1996. *In vitro* function and durability of a polyurethane heart valve: material considerations. Journal of Heart Valve Disease 5 (5), 538–542.

Bernacca, G.M., Mackay, T.G., Wilkinson, R., Wheatleym, D.J., 1997. Polyurethane heart valves: fatigue failure, calcification and polyurethane structure. Journal of Biomedical Materials Research 34 (3), 371–379.

Bernacca, G.M., Straub, I., Wheatley, D.J., 2002. Mechanical and morphological study of biostable polyurethane heart valve leaflets explanted from sheep. Journal of Biomedical Materials Research 61 (1), 138–145.

Bernacca, G.M., McColl, J.H., Wheatley, D.J., 2004. Comparison of prosthetic valve hydrodynamic function: objective testing using statistical multilevel modeling. Journal of Heart Valve Disease 13 (3), 467–477.

Berne, R.M., Levy, M.N., 1986. Cardiovascular Physiology. Mosby, St. Louis.

Chen, L., McCulloch, A.D., May-Newman, K., 2004. Nonhomogeneous deformation in the anterior leaflet of the mitral valve. Annals of Biomedical Engineering 32 (12), 1599–1606.

Christie, G.W., 1992. Computer modelling of bioprosthetic heart valves. European Journal of Cardio-Thoracic Surgery 6 (Suppl. 1), S95–S101.

Cochran, R.P., Kunzelman, K.S., 1998. Effect of papillary muscle position on mitral valve function: relationship to homografts. Annals of Thoracic Surgery 66 (6, Suppl.), S155–S161.

Daebritz, S.H., Sachweh, J.S., Hermanns, B., Fausten, B., Franke, A., Groetzner, J., Klosterhalfen, B., Messmer, B.J., 2003. Introduction of a flexible polymeric heart valve prosthesis with special design for mitral position. Circulation 108 (10), 134–139.

Einstein, D.R., Kunzelman, K.S., Reinhall, P.G., Nicosia, M.A., Cochran, R.P., 2005. Non-linear fluid coupled computational model of the mitral valve. Journal of Heart Valve Disease 14 (3), 376–385.

Fauci, L.J., Peskin, C.S., 1988. A computational model of aquatic animal locomotion. Journal of Computational Physics 77 (1), 85–108.

Fisher, J., Jack, G.R., Wheatley, D.J., 1986. Design of a function test apparatus for prosthetic heart valves: initial results in the mitral position. Clinical Physics and Physiological Measurement 7 (1), 63–73.

Grashow, J.S., Yoganathan, A.P., Sacks, M.S., 2006. Biaxial stress–stretch behavior of the mitral valve anterior leaflet at physiologic strain rates. Annals of Biomedical Engineering 34 (2), 315–325.

He, Z.M., Sacks, M.S., Baijens, L., Wanant, S., Shah, P., Yoganathan, A.P., 2003. Effects of papillary muscle position on *in-vitro* dynamic strain on the porcine mitral valve. Journal of Heart Valve Disease 12 (4), 488–494.

He, Z.M., Ritchie, J., Grashow, J.S., Sacks, M.S., Yoganathan, A.P., 2005. *In vitro* dynamic strain behaviour of the mitral valve posterior leaflet. Journal of Biomechanical Engineering 127 (3), 504–511.

Komeda, M., De Anda, A., Glasson, J.R., Daugthers, G.T., Bolger, A.F., Nikolic, S.D., Ingels, N.B., Miller, C., 1996a. Improving methods of chordal-sparing mitral valve replacement—Part II: optimal tension for chordal resuspension. Journal of Heart Valve Disease 5 (5), 477–483.

Komeda, M., De Anda, A., Glasson, J.R., Daugthers, G.T., Bolger, A.F., Nikolic, S.D., Ingels, N.B., Miller, C., 1996b. Improving methods of chordal-sparing mitral valve replacement—Part III: optimal direction for artificial chordae. Journal of Heart Valve Disease 5 (5), 484–490.

Kunzelman, K.S., Cocharan, M.D., 1993. Finite element analysis of the mitral valve. Journal of Heart Valve Disease 2 (3), 326–340.

Kunzelman, K.S., Cochran, R.P., Verrier, E.D., 1993a. Finite element analysis of mitral valve pathology. Journal of Long-Term Effects of Medical Implants 3 (3), 161–179.

Kunzelman, K.S., Cochran, R.P., Murphree, S.S., Ring, W.S., Verrier, E.D., Eberhart, R.C., 1993b. Differential collagen distribution in the mitral valve and its influence on biomechanical behaviour. Journal of Heart Valve Disease 2 (2), 236–244.

Kunzelman, K.S., Reimink, M.S., Cochran, R.P., 1997. Annular dilatation increases stress in the mitral valve and delays coaptation: a finite element computer model. Cardiovascular Surgery 5 (4), 427–434.

Kunzelman, K.S., Reimink, M.S., Cochran, R.P., 1998a. Flexible versus rigid ring annuloplasty for mitral valve annular dilatation: a finite element model. Journal of Heart Valve Disease 7 (1), 108–116.

Kunzelman, K.S., Quick, D.W., Cochran, R.P., 1998b. Altered collagen concentration in mitral valve leaflets: biochemical and finite element analysis. Annals of Thoracic Surgery 66 (6, Suppl.), S198–S205.

Liao, J., Vesely, I., 2003. A structural basis for the size-related mechanical properties of mitral valve chordae tendineae. Journal of Biomechanics 36 (8), 1125–1133.

Lim, K.H., Yeo, J.H., Duran, C.M.G., 2005. Three dimensional asymmetrical modeling of the mitral valve: a finite element study with dynamic boundaries. Journal of Heart Valve Disease 14 (3), 386–392.

Liu, Y.R., Kasyanov, V., Schoephoerster, R.T., 2007. Effect of fiber orientation on the stress distribution within a leaflet of a polymer composite heart valve in the closed position. Journal of Biomechanics 40, 1099–1106.

Mackay, T.G., 1992. Towards a tri-leaflet polyurethane heart valve prosthesis. Ph.D. Thesis, University of Strathclyde, Thesis no. T7473.

Mackay, T.G., Bernacca, G.M., Wheatley, D.J., Fisher, A.C., Hindle, C.S., 1996. *In vitro* function and durability assessment of a polyurethane heart valve prosthesis. International Journal of Artificial Organs 20, 1017–1025.

Marzilli, M., Sabbah, H.N., Lee, T., Stein, P.D., 1980. Role of the papillary muscle in opening and closure of the mitral valve. American Journal of Physiology: Heart and Circulatory Physiology 238, H348–H354.

Ming, L., Zhen, H.K., 1986. Study of the closing mechanism of natural heart valves. Applied Mathematics and Mechanics 7, 955–964.

McQueen, D.M., Peskin, C.S., 1997. Shared-memory parallel vector implementation of the immersed boundary method for the computation of blood flow in the beating mammalian heart. Journal of Supercomputing 11 (3), 213–236.

Peskin, C.S., 1972. Flow patterns around heart valves: a numerical method. Journal of Computational Physics 10, 252–271.

Peskin, C.S., 1977. Numerical analysis of blood flow in the heart. Journal of Computational Physics 25, 220–252.

Peskin, C.S., 2002. The immersed boundary method. Acta Numerica 11, 479–517.

Peskin, C.S., McQueen, D.M., 1989. A three dimensional computational method for blood flow in the heart I. Immersed elastic fibres in a viscous incompressible fluid. Journal of Computational Physics 81 (2), 372–405.

Peskin, C.S., McQueen, D.M., 1995. A general method for the computer simulation of biological systems interacting with fluids. Symposia of the Society for Experimental Biology 49, 265–276.

Peskin, C.S., McQueen, D.M., 1996. Fluid dynamics of the heart and its valves. In: Othmer, H.G., Adler, F.R., Lewis, M.A., Dallon, J.C. (Eds.), Case Studies in Mathematical Modeling: Ecology, Physiology, and Cell Biology. Prentice-Hall, Englewood Cliffs, NJ, pp. 309–337.

Pierrakos, O., Vlachos, P.P., 2006. The effect of vortex formation on left ventricular filling and mitral valve efficiency. Journal of Biomechanical Engineering 128 (4), 527–539.

Redaelli, A., Guadagni, G., Fumero, R., 2001. A computational study of the hemodynamics after "Edge-to-Edge" mitral valve repair. Journal of Biomechanical Engineering 123 (6), 565–570.

Reimink, M.S., Kunzelman, K.S., Cochran, R.P., 1996. The effect of chordal replacement suture length on function and stresses in repaired mitral valves: a finite element study. Journal of Heart Valve Disease 5 (4), 365–375.

Reul, H., Talukder, N., Muller, E.W., 1981. Fluid mechanics of the natural mitral valve. Journal of Biomechanics 14, 361–372.

Ritchie, J., Jiminez, J., He, Z., Sacks, M.S., Yoganathan, A.P., 2006. The material properties of the native porcine mitral valve chordae tendineae: an *in vitro* investigation. Journal of Biomechanics 39 (6), 1129–1135.

Saber, N.R., Gosman, A.D., Wood, N.B., Kilner, P.J., Charrier, C.L., Firmin, D.N., 2001. Computational flow modelling of the left ventricle based on *in vivo* MRI data: initial experience. Annals of Biomedical Engineering 29 (4), 275–283.

Sacks, M.S., He, Z., Baijens, L., Wanant, S., Shah, P., Sugimoto, H., Yoganathan, A.P., 2002. Surface strains in the anterior leaflet of the functioning mitral valve. Annals of Biomedical Engineering 30 (10), 1281–1290.

van Rijk-Zwikker, G.L., Delemarre, B.J., Huysmans, H.A., 1994. Mitral valve anatomy and morphology: relevance to mitral valve replacement and reconstruction. Journal of Cardiac Surgery 9 (2, Suppl.), 255–261.

Vesely, I., 2003. The evolution of bioprosthetic heart valve design and its impact on durability. Cardiovascular Pathology 12, 277–286.

Watton, P.N., Luo, X.Y., Bernacca, G.M., Molloy, P., Wheatley, D.J., 2007. Dynamic modelling of prosthetic chorded mitral valves. Journal of Biomechanics 40 (3), 613–626.

Wheatley, D.J., 2002. Mitral valve prosthesis. Patent number WO03037227.

Wheatley, D.J., Raco, L., Bernacca, G.M., Sim, I., Belcher, P.R., Boyd, J.S., 2000. Polyurethane: material for the next generation of heart valve prostheses? European Journal of Cardio-Thoracic Surgery 17, 440–447.

Yoganathan, A.P., 2000. Cardiac Valve Prosthesis. In: Bronzino, J.D. (Ed.), The Biomedical Engineering Handbook, Vol. 2, CRC Press, Boca Raton, FL.

Yoganathan, A.P., Chandran, K.B., Sotiropoulos, F., 2005. Flow in prosthetic heart valves: state-of-art and future directions. Annals of Biomedical Engineering 33 (12), 1689–1694.